Draft version August 16, 2016
Preprint typeset using LaTeX style AASTeX6 v. 1.0

arXiv:1608.03896v1 [astro-ph.HE] 12 Aug 2016

ON HELIUM MIXING IN QUASI-GLOBAL SIMULATIONS OF THE INTRACLUSTER MEDIUM

Thomas Berlok[1] and Martin E. Pessah[1]
[1]Niels Bohr International Academy, Niels Bohr Institute, Blegdamsvej 17, DK-2100 Copenhagen Ø, Denmark; berlok@nbi.dk mpessah@nbi.dk

ABSTRACT

The assumption of a spatially uniform helium distribution in the intracluster medium can lead to biases in the estimates of key cluster parameters if composition gradients are present. The helium concentration profile in galaxy clusters is unfortunately not directly observable. Current models addressing the putative sedimentation are one-dimensional and parametrize the presence of magnetic fields in a crude way, ignoring the weakly-collisional, magnetized nature of the medium. When these effects are considered, a wide variety of instabilities can play an important role in the plasma dynamics. In a series of recent papers, we have developed the local, linear theory of these instabilities and addressed their non-linear development with a modified version of Athena. Here, we extend our study by developing a quasi-global approach that we use to simulate the mixing of helium as induced by generalizations of the heat-flux-driven buoyancy instability (HBI) and the magneto-thermal instability (MTI), which feed off thermal and composition gradients. In the inner region of the ICM, mixing can occur on few Gyrs, after which the average magnetic field inclination angle is $\sim 30-50^\circ$ resulting in an averaged Spitzer parameter higher by about 20% than the value obtained in homogeneous simulations. In the cluster outskirts the instabilities are rather inefficient, due to the shallow gradients. This suggests that compositions gradients in cluster cores might be shallower than one-dimensional models predict. More quantitative statements demand more refined models that can incorporate the physics driving the sedimentation process and simultaneously account for the weakly-collisional nature of the plasma.

Keywords: galaxies: clusters: intracluster medium — instabilities — magnetohydrodynamics — diffusion

1. INTRODUCTION

The intracluster medium (ICM) of galaxy clusters is comprised of a very high temperature and low density gas in which charged particles are bound to the magnetic field with gyroradii that are much smaller than the mean free path of particle collisions. In this weakly collisional medium, the weak ($\sim \mu$G) magnetic field (Carilli & Taylor 2002) channels the transport of heat and momentum, as well as the diffusion of particles. The anisotropic character of the weakly-collisional ICM has been found to significantly alter its dynamical properties. Whereas the stability of a stratified gas in the presence of a gravitational field is governed by its entropy gradient (Ledoux 1947; Schwarzschild 1958), Balbus (2000, 2001) and Quataert (2008) found that temperature gradients can have an important impact on the stability properties if the plasma is weakly collisional. Two distinct instabilities were found to feed off temperature gradients in weakly-collisional plane-parallel atmospheres, even when their entropy increases with height. The discovery of the magneto-thermal instability (MTI, Balbus 2000, 2001), maximally unstable when the magnetic field is perpendicular to gravity and the temperature decreases with height and the heat-flux-driven buoyancy instability (HBI, Quataert 2008), maximally unstable when the magnetic field is parallel to gravity and the temperature increases with height, led to a surge in research on the stability properties of the ICM during the last decade.

These investigations considered both two and three-dimensional simulations in local, quasi-global, and even global settings including a variety of physical effects, for instance, anisotropic heat conduction, Braginskii viscosity, radiative cooling and imposed turbulence (Parrish & Stone 2005, 2007; Parrish & Quataert 2008; Parrish et al. 2008, 2009; Bogdanović et al. 2009; Parrish et al. 2010; Ruszkowski & Oh 2010; McCourt et al. 2011, 2012; Kunz et al. 2012; Parrish et al. 2012a,b). This collection of studies have led to a better understanding of a number of fundamental issues governing ICM plasma dynamics (see Balbus & Potter (2016) for a recent review of the physics of the MTI and HBI). In particular, Kunz (2011) pointed out that Braginskii viscosity makes the fastest growing wavelengths for the HBI very long in the direction parallel to gravity (see also Gupta et al. 2016). This limited the validity of the local approaches employed thus far and ultimately led to quasi-global studies of the HBI (Latter & Kunz 2012; Kunz et al. 2012).

While the temperature distribution of the ICM is observable (Vikhlinin et al. 2006), the fact that most elements are completely ionized makes it difficult to constrain the com-

position of the plasma. If present, composition gradients, as envisioned for example by the sedimentation of helium over a Hubble time, can lead to biases in the estimates of key cluster properties with important implications for cosmology (Markevitch 2007; Peng & Nagai 2009). This has motivated the study of the long-term dynamics of heavy elements in the ICM. As an example, the models in Peng & Nagai (2009) predict that composition gradients can lead to a bias of up to 20 percent in the Hubble constant if the total mass of the cluster is estimated assuming a uniform, primordial composition (see Figure 4 in Peng & Nagai 2009). The models for the evolution of the radial distribution of elements are one-dimensional (Fabian & Pringle 1977; Gilfanov & Syunyaev 1984; Chuzhoy & Nusser 2003; Chuzhoy & Loeb 2004; Peng & Nagai 2009; Shtykovskiy & Gilfanov 2010) and consider the effects of magnetic fields in rather simplified form, or ignore it altogether.

Motivated by the need of a more fundamental approach to understand the role of magnetic fields in the dynamics of weakly-collisional media Pessah & Chakraborty (2013) and Berlok & Pessah (2015) extended the works carried out in homogeneous settings by Balbus (2000, 2001), Quataert (2008) and Kunz (2011) to include composition gradients. They showed that a host of instabilities feeding off composition gradients can have an important impact on the stability properties of the ICM. Two of these instabilities are the generalizations of the MTI and HBI, namely the magneto-thermo-compositional instability (MTCI) and the heat- and particle-flux-driven buoyancy instability (HPBI). Both instabilities can be active even for isothermal atmospheres if the mean molecular weight increases with height, even if the entropy gradient increases with height.

In order to understand how the new instabilities driven by composition gradients saturate, Berlok & Pessah (2016) considered the non-linear evolution of the MTCI and the HPBI in local, isothermal settings, using a modified version of the magnetohydrodynamics (MHD) code Athena (Stone et al. 2008). These simplifying assumptions made it possible to understand some of the differences observed in the saturated state of instabilities that are driven by either thermal or composition gradients alone. A notable difference is that the instabilities driven exclusively by composition gradients saturate with an average magnetic field inclination of 45°. This is in contrast to the thermal instabilities where the MTI drives the magnetic field to be almost parallel to gravity (Parrish & Stone 2005) and the HBI drives the magnetic field to be almost perpendicular to gravity (Parrish & Quataert 2008). If composition gradients can prevent the saturated field in the inner cluster to be perpendicular to the radial direction under more general circumstances, this could potentially help to alleviate the thermal insulation thought to be a consequence of the HBI in homogeneous media (Parrish & Quataert 2008; Bogdanović et al. 2009; Parrish et al. 2009; Kunz et al. 2012).

In this paper, we present the first two-dimensional (2D) quasi-global simulations of plane-parallel atmospheres with initial equilibrium structures inspired by the models of Peng & Nagai (2009), that we use to model the inner and outer regions of the ICM. We show that the HPBI leads to mixing of the helium content in the inner regions of the ICM and, as a consequence, diminishes the initial gradient in composition. The inclusion of a composition gradient leads to a $\sim$ 20 % increase in heat flux to the core at late times compared with a simulation of a homogeneous ICM. Our simulations therefore illustrate that composition gradients could play a role in determining to what extent the core is thermally shielded from its surroundings.

The paper is organized as follows: In Section 2, we introduce the equations of kinetic MHD that we employ to model a completely ionized plasma composed of hydrogen and helium. In Section 3, we present an equilibrium atmosphere for the inner regions of the ICM which is based on the helium sedimentation model of Peng & Nagai (2009). This atmosphere is then studied in Section 4 by using a quasi-global linear theory and in Section 5 by performing a suite of simulations using a modified version of the MHD code Athena (Stone et al. 2008; Berlok & Pessah 2016). We also present in Section 6 simulations of the outer region of the ICM, where the MTCI could be active. We conclude in Section 7 by discussing the consequences of plasma instabilities on the longterm evolution of composition gradients in the ICM as well as the limitations of our present approach.

2. KINETIC MHD FOR A BINARY MIXTURE

We model the intracluster medium by solving equations that evolve the total mass density, ρ, momentum density, $\rho\boldsymbol{v}$, magnetic field, $\boldsymbol{B}$, total energy density, E, and composition, c, for a weakly collisional binary mixture of hydrogen and helium. Here, $\boldsymbol{v}$ is the fluid velocity and the total energy density of the plasma is given by

$$E = \frac{1}{2}\rho v^2 + \frac{B^2}{8\pi} + \frac{P}{\gamma - 1}\,, \tag{1}$$

where $\gamma = 5/3$ is the adiabatic index and P is the thermal gas pressure. We assume the magnetic field to have direction $\hat{\boldsymbol{b}} = (b_x, 0, b_z)$ and define the composition of the plasma as

$$c \equiv \frac{\rho_{\rm He}}{\rho}\,. \tag{2}$$

The plasma is assumed to obey the ideal gas law

$$P = \frac{\rho k_{\rm B} T}{\mu m_{\rm H}}\,, \tag{3}$$

where T is the temperature, $m_{\rm H}$ is the proton mass and $k_{\rm B}$ is Boltzmann's constant. The mean molecular weight, μ, which enters in Equation (3), can be shown to be related to the composition by

$$\mu = \frac{4}{8 - 5c}\,, \tag{4}$$

for a completely ionized mixture of hydrogen and helium.

The equations of motion are (Pessah & Chakraborty 2013; Berlok & Pessah 2016): the continuity equation for the total mass

$$\frac{\partial \rho}{\partial t} + \nabla\cdot(\rho \boldsymbol{v}) = 0\,, \tag{5}$$

the momentum equation

$$\frac{\partial (\rho \boldsymbol{v})}{\partial t} + \nabla\cdot\left(\rho \boldsymbol{v}\boldsymbol{v} + P_{\rm T}\mathsf{I} - \frac{B^2}{4\pi}\hat{\boldsymbol{b}}\hat{\boldsymbol{b}}\right) = -\nabla\cdot\Pi + \rho \boldsymbol{g}, \tag{6}$$

the energy equation

$$\frac{\partial E}{\partial t} + \nabla\cdot\left[(E + P_{\rm T})\,\boldsymbol{v} - \frac{\boldsymbol{B}\,(\boldsymbol{B}\cdot\boldsymbol{v})}{4\pi}\right] = -\nabla\cdot\boldsymbol{Q}_{\rm s} - \nabla\cdot(\Pi\cdot\boldsymbol{v}) + \rho\boldsymbol{g}\cdot\boldsymbol{v}\,, \tag{7}$$

the induction equation for the magnetic field

$$\frac{\partial \boldsymbol{B}}{\partial t} = \nabla\times(\boldsymbol{v}\times\boldsymbol{B})\,, \tag{8}$$

and the continuity equation for the helium mass

$$\frac{\partial (c\rho)}{\partial t} + \nabla\cdot(c\rho\boldsymbol{v}) = -\nabla\cdot\boldsymbol{Q}_{\rm c}\,. \tag{9}$$

In these equations, $P_{\rm T}$ is the total pressure (gas + magnetic) and $\boldsymbol{g} = (0, 0, -g)$ is the gravitational acceleration which we assume to be constant.

The equations include terms that take into account the influence of three anisotropic effects. These anisotropic effects arise because the plasma is weakly collisional and weakly magnetised. In this regime the charged particles are effectively bound to the magnetic field and collisions occur primarily along the magnetic field. This makes the assosicated transport phenomena be directed along the magnetic field.

Electrons, which are responsible for heat conduction, can in this way create a heat flux along the magnetic field given by

$$\boldsymbol{Q}_s = -\chi_{\parallel}\hat{\boldsymbol{b}}\hat{\boldsymbol{b}}\cdot\nabla T, \tag{10}$$

where $\chi_{\parallel}$ is the Spitzer heat conductivity (Spitzer 1962).

Similarly, the continuity equation for the helium density includes a flux of composition along the magnetic field given by (Bahcall & Loeb 1990; Pessah & Chakraborty 2013)

$$\boldsymbol{Q}_c = -D\hat{\boldsymbol{b}}\hat{\boldsymbol{b}}\cdot\nabla c\,, \tag{11}$$

where D is the diffusion coefficient.

Finally, conservation of the first adiabatic invariant of the ions can lead to anisotropy in the pressure tensor with differences in the parallel ($p_{\parallel}$) and perpendicular ($p_{\perp}$) pressures. This pressure difference results in gradients in velocity-components along the magnetic field being viscously damped. This effect, called Braginskii viscosity (Braginskii 1965), is described by the viscosity tensor

$$\Pi = -3\rho\nu_{\parallel}\left(\hat{\boldsymbol{b}}\hat{\boldsymbol{b}} - \frac{1}{3}\mathbf{I}\right)\left(\hat{\boldsymbol{b}}\hat{\boldsymbol{b}} - \frac{1}{3}\mathbf{I}\right):\nabla\boldsymbol{v}\,, \tag{12}$$

where $\nu_{\parallel}$ is the viscosity coefficient and $\mathbf{I}$ is a unit tensor.

Expressions for the dependence of $\chi_{\parallel}$, D and $\nu_{\parallel}$ for an ionized mixture of hydrogen and helium can be found in the Appendix of Berlok & Pessah (2015). More details about the utility of Braginskii MHD and its range of applicability can be found in Schekochihin et al. (2005); Kunz et al. (2012); Pessah & Chakraborty (2013) and references therein.

For future reference we also define the plasma-$\beta = 8\pi P/B^2 = 2v_{\rm th}^2/v_{\rm A}^2$, where $v_{\rm A} = B/\sqrt{4\pi\rho}$ is the Alfvén speed and $v_{\rm th} = \sqrt{P/\rho}$ is the thermal speed.

3. EQUILIBRIUM PROFILE

In order to understand the quasi-global linear dynamics arising from Equations (5-9), we derive an equilibrium profile for a model plane parallel atmosphere, which has proven to be useful for capturing key aspects of the plasma dynamics in galaxy clusters. We assume that gravity can be modelled locally via a constant acceleration, g, and that the magnetic field is purely vertical, i.e., $b_x = 0$ and $b_z = 1$. The magnetic field is assumed to be weak enough that we can neglect its contribution to the total pressure gradient responsible for hydrostatic equilibrium. Nevertheless, the vertical weak magnetic field can enable a background heat flux in the vertical direction. Therefore, in order for the model atmosphere to be in equilibrium we require $\nabla\cdot\boldsymbol{Q}_c = 0$ and $\nabla\cdot\boldsymbol{Q}_c = 0$. In what follows, we ignore helium diffusion and assume $D = 0$ such that the second condition is trivially satisfied.

Motivated by the models considered in Peng & Nagai (2009), which result in helium concentration profiles that peak off-center, we consider a situation where the composition of the plasma increases linearly outwards from the bottom of the atmosphere, i.e., center of the cluster, as

$$c\,(z) = c_0 + s_{\rm c} z\,, \tag{13}$$

where $s_{\rm c} = (c_Z - c_0)/L_Z$ is the slope in composition. Notice that the mass concentration of helium, $c(z)$, is related to the mean molecular weight, $\mu(z)$, by

$$\mu(z) = \frac{4}{8 - 5c(z)}\,, \tag{14}$$

for a completely ionized plasma of hydrogen and helium. The equilibrium needs to fulfill

$$\frac{d}{dz}\left(\chi_{\parallel}\frac{dT}{dz}\right) = 0\,, \tag{15}$$

where $\chi_{\parallel}$ is a function of temperature $T(z)$ and composition, $c(z)$. We will for simplicity assume that $\chi_{\parallel}$ depends only on temperature as $\chi_{\parallel} = \chi_{\parallel,0}(T/T_0)^{5/2}$, i.e. we assume that the dependence on composition can be neglected[1]. With this assumption, Equation (15) is identical to the one derived in

[1] For the profiles employed here, the dependence on composition is much weaker than the dependence on temperature (Pessah & Chakraborty 2013). The maximum error incurred by using this approximation is less than 5 % on the value of $\chi_{\parallel}$ at the top of the atmosphere.

Latter & Kunz (2012) and it decouples from the rest of the equations yielding the solution

$$T(z) = T_0\,(1+\zeta z)^{2/7}\ , \tag{16}$$

where $\zeta L_Z = (T_Z/T_0)^{7/2} - 1$ and T_Z (T_0) is the temperature at the top (bottom) of the atmosphere. Using the equation of state

$$P(z) = \frac{\rho(z)\,k_{\rm B}T(z)}{\mu(z)\,m_{\rm H}}\ , \tag{17}$$

we solve the equation for hydrostatic equilibrium

$$\frac{\partial P}{\partial z} = -\rho g\ , \tag{18}$$

and find

$$P(z) = P_0 e^{h(0)-h(z)}\ , \tag{19}$$

where the function $h(z)$ is related to a Gauss hypergeometric function, ${}_2F_1$, as

$$h(z) = \frac{28(1+\zeta z)^{5/7}}{5H_0\alpha}\ {}_2F_1\left(\frac{5}{7},1;\frac{12}{7};\frac{5s_{\rm c}\mu_0}{\alpha}(1+\zeta z)\right). \tag{20}$$

In deriving the above result we have introduced the scale height at the bottom of the atmosphere

$$H_0 = \frac{k_{\rm B}T_0}{\mu_0 m_{\rm H} g}\ , \tag{21}$$

and the parameter

$$\alpha = 5s_{\rm c}\mu_0 + 4\zeta\ . \tag{22}$$

The density, $\rho(z)$, can then be found from Equation (3).

The values of the constants used for this equilibrium atmosphere are inspired by the model of Peng & Nagai (2009). In physical units, the model atmosphere has height $L_Z = 2H_0 =$ 80 kpc, corresponding to the region between $r/r_{500} = 0.01$ and $r/r_{500} = 0.06$ with $r_{500} = 1.63$ Mpc in their model. The values for the temperature and composition of the plasma at the top and bottom of the atmosphere are given by $T_Z = 9.6$ keV, $T_0 = 5.8$ keV, $c_Z = 0.62$, and $c_0 = 0.52$, respectively. In Figure 1 we show $P(z)/P_0$, $\rho(z)/\rho_0$, $T(z)/T_0$, $\mu(z)/\mu_0$ and $(2H_0m_{\rm H}/3k_{\rm B})\,(ds/dz)$, where the entropy per unit mass is defined by

$$s = \frac{3k_{\rm B}}{2m_{\rm H}}\ln\left[\left(\frac{P}{P_0}\right)\left(\frac{\rho}{\rho_0}\right)^{-5/3}\right]\ . \tag{23}$$

Note that, even though the composition increases with height, the Ledoux criterion for stability (Ledoux 1947) (which is the generalization of the Schwarzschild criterion, Schwarzschild 1958, valid for a heterogeneous collisional medium) is not violated. Indeed, for this model atmosphere the entropy is an increasing function of height, i.e.,

$$\frac{ds}{dz} > 0\ , \tag{24}$$

as illustrated in Figure 1. As we will discuss next, the instabilities present in the linear theory and in the simulations are due to the weakly collisional nature of the plasma.

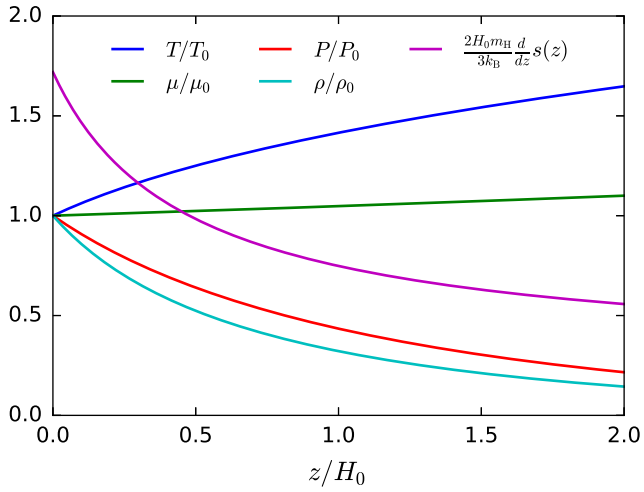

Figure 1. Equilibrium atmosphere inspired by the sedimentation model of Peng & Nagai (2009) and the radial temperature profile of Vikhlinin et al. (2006). The temperature (blue) and the mean molecular weight (green) increase with radius while pressure (red) and density (magenta) decrease with radius at this radial distance in the cluster model. The derivative of the entropy (purple) is positive, indicating stability according to Equation (24).

4. QUASI-GLOBAL LINEAR THEORY

The HPBI has its fastest growth rates on radial scales longer than a scale height when Braginskii viscosity is included in the analysis (Berlok & Pessah 2015). The local linear mode analysis is therefore not strictly valid as it assumes that the radial scales are much shorter than a scale height. This problem has previously been found for the HBI in Kunz (2011) and solved by introducing a quasi-global linear theory for the HBI in Latter & Kunz (2012). In the same vein, in this section, we develop a quasi-global linear theory for the HPBI by considering a model atmosphere with a non-uniform mean molecular weight.

The purpose of deriving a quasi-global theory is to predict the growth rates of the instability as a function of perpendicular wavenumber, k_x, in order to understand whether the instability will grow on astrophysically relevant timescales. Furthermore, the eigenmodes obtained from linear theory can also be used to compare with the linear stage of simulations using Athena. Such a comparison will serve as a test of our modified version of Athena in Section 4.3.

4.1. *Equations of Motion and Relevant Parameters*

The equations governing the quasi-global, linear dynamics for the perturbations are obtained from the equations of kinetic MHD for a binary mixture (Pessah & Chakraborty 2013; Berlok & Pessah 2015) by using a Fourier transform along the x-coordinate but retaining the z-derivatives explicitly in order to relax the local approximation. Therefore, the perturbations are calculated in terms of the complex Fourier coefficients, $\tilde{f}(k_x, z)$, which we assume to have a time dependence, $\exp(\sigma t)$, where σ is the (in general complex) eigenvalue. We assume that $\chi_\parallel = \chi_{\parallel,0}(T/T_0)^{5/2}$ and

$\nu_\parallel = \nu_{\parallel,0}\,\rho_0/\rho\,(T/T_0)^{5/2}$, i.e. $\chi_\parallel$ and $\nu_\parallel$ only depend on the composition through the constants $\chi_{\parallel,0}$ and $\nu_{\parallel,0}$. We also introduce a flux function such that $\boldsymbol{B} = \nabla \times (A\hat{\boldsymbol{y}})$. The initial condition is $A = Bx$ which is equivalent to $\boldsymbol{B} = B\hat{\boldsymbol{z}}$. In the present work, we only consider the case of $D = 0$. In this case, and with the above caveats, the quasi-global linearized equations are: the continuity equation

$$\sigma\frac{\delta\rho}{\rho} = -ik_x\delta v_x - \left(\frac{d\ln\rho}{dz} + \frac{\partial}{\partial z}\right)\delta v_z, \tag{25}$$

the x-component of the momentum equation

$$\sigma\delta v_x = -ik_x\frac{T}{\mu}\left(\frac{\delta\rho}{\rho} + \frac{\delta T}{T} - \frac{\delta\mu}{\mu}\right) + \frac{2}{\rho\beta_0}\left(k_x^2 - \frac{\partial^2}{\partial z^2}\right)\delta A - \frac{ik_xT^{5/2}}{3\rho\,\mathrm{Re}_0}\left(2\frac{\partial\delta v_z}{\partial z} - ik_x\delta v_x\right), \tag{26}$$

the z-component of the momentum equation

$$\sigma\delta v_z = -\frac{T}{\mu}\left(\frac{\delta T}{T} - \frac{\delta\mu}{\mu}\right)\frac{d\ln P}{dz} - \frac{T}{\mu}\frac{\partial}{\partial z}\left(\frac{\delta\rho}{\rho} + \frac{\delta T}{T} - \frac{\delta\mu}{\mu}\right) + \frac{2T^{5/2}}{3\rho\mathrm{Re}_0}\left(\frac{5}{2}\frac{d\ln T}{dz} + \frac{\partial}{\partial z}\right)\left(2\frac{\partial\delta v_z}{\partial z} - ik_x\delta v_x\right), \tag{27}$$

the entropy equation (with $\gamma = 5/3$)

$$\frac{3}{2}\sigma\frac{\delta T}{T} = -ik_x\delta v_x - \left(\frac{3}{2}\frac{d\ln T}{dz} + \frac{\partial}{\partial z}\right)\delta v_z + \frac{1}{P\,\mathrm{Pe}_0}\left(\frac{\partial^2}{\partial z^2}\left(T^{7/2}\frac{\delta T}{T}\right) + q_0ik_x\frac{\partial\delta A}{\partial z}\right), \tag{28}$$

the induction equation

$$\sigma\delta A = -\delta v_x\,, \tag{29}$$

and the equation for the mean molecular weight, μ,

$$\sigma\frac{\delta\mu}{\mu} = -\delta v_z\frac{d\ln\mu}{dz}. \tag{30}$$

Here, the perturbation to the flux function is related to the perturbation to the magnetic field by $\delta\boldsymbol{B} = \nabla\times(\delta A\,\hat{\boldsymbol{y}})$.

Equations (25-30) have been written in dimensionless variables by scaling μ with μ_0, T with T_0, the velocities with $v_{\mathrm{th},0}$, σ with $\sigma_0 = t_0^{-1} = v_{\mathrm{th},0}/H_0$, δA with B_0H_0 and z with H_0 such that k_x is scaled with $1/H_0$. The background heat flux parameter q_0, is given by

$$q_0 = -T^{7/2}\frac{d\ln T}{dz}\,, \tag{31}$$

in dimensionless variables. At the bottom of the atmosphere, $z = 0$, the Peclet number is given by

$$\mathrm{Pe}_0 = \frac{v_{\mathrm{th},0}\,P_0\,H_0}{\chi_{\parallel,0}\,T_0} \approx 70\,, \tag{32}$$

and the Reynolds number is given by

$$\mathrm{Re}_0 = \frac{v_{\mathrm{th},0}\,\rho_0\,H_0}{\nu_{\parallel,0}} \approx 3800\,. \tag{33}$$

These parameters were found by using Equations (B6) and (B7) in Berlok & Pessah (2015) to estimate the values of $\chi_{\parallel,0}$ and $\nu_{\parallel,0}$. Following Latter & Kunz (2012) and Kunz et al. (2012) we furthermore take the plasma-β at the bottom of the atmosphere to be

$$\beta_0 = 10^5\,. \tag{34}$$

4.2. *Solutions obtained with a pseudo-spectral method*

The linearized quasi-global equations (Equations 25-30) are solved using a pseudo- spectral method, in a manner similar to the analysis presented in Latter & Kunz (2012), see also Boyd (2000). We discretize the six equations on a Chebyshev-Gauss-Lobatto roots grid transformed onto the domain $z = [0, 2]$. The grid has N grid points, where $N = 200$, and the resulting algebraic equations constitute a generalized eigenvalue problem of size $6N$. We use the same boundary conditions as Latter & Kunz (2012) which means that δv_z, $\delta T/T$, and $\partial_z\delta A$ are set to zero at the boundaries. The latter condition corresponds to $\delta B_x = 0$ at the boundaries, which implies that the field remains vertical there. We furthermore impose $\delta\mu/\mu = 0$ at the boundaries.

Equations (25)-(30) only depend on the value of $k_xH_0 = 2\pi n$ where n is the horizontal mode number. All other parameters are set by our model. For each value of k_x, there are a number of modes which we designate with the vertical mode number m, where $m = 1$ is the fastest growing mode, $m = 2$ labels the second fastest growing mode, and so on. We show the solution for $n = 5$ in Figure 2, where the left panel shows the $m = 1$ mode which is confined to the lower region of the domain. The right panel shows the $m = 2$ mode which has a slower growth rate but a larger vertical extent than the $m = 1$ mode. This is a general property of the solutions: The vertical extent of the perturbations increase with the mode number m, while it does not depend on the mode number n. Therefore, in a simulation where the instability is excited using Gaussian noise, we expect the perturbations to grow fastest in the lower region of the computational domain. This is indeed the case, as we will see in Section 5.

The growth rates as a function of the wavenumber, k_x, are shown in Figure 3, where the solid lines are obtained using the pseudo-spectral method and the crosses are obtained from Athena simulations (see next subsection). The maximum growth rate is $\sigma_{\max} \approx 10\ \mathrm{Gyr}^{-1}$ implying that the instability can develop significantly on relevant time scales. The gradient in the mean molecular weight acts to increase the growth rate with respect to the homogeneous case. The maximum growth rate found for the HPBI is however still smaller than the one found for the HBI in Latter & Kunz (2012) due to the shallower temperature gradient that we use in this work, which is inspired by the models in Peng & Nagai (2009) as detailed above. The temperature ratio, T_Z/T_0, is 2.5 in the model of Latter & Kunz (2012) while it is only ~ 1.65 in our model. The growth rate is proportional to the gradient in temperature in the local, weak magnetic field and fast heat conduction limit. A rough estimate is therefore that their growth rate should be higher by a factor of roughly 1.5, which we

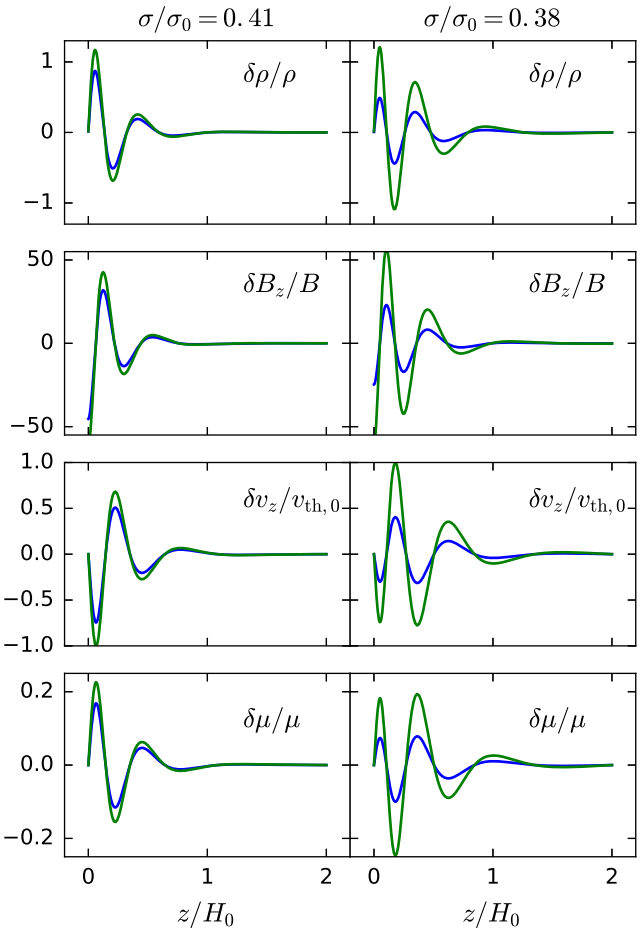

Figure 2. Select components of the eigenmode for the fastest (left, $m = 1$) and second fastest (right, $m = 2$) eigenmode with $n = 5$ and the real (imaginary) part of the eigenmode shown in blue (green). A general rule seems to be that the fastest growing modes have a small vertical extent while slower growing modes have a larger vertical extent. This trend also appears in the homegeneous setting (Latter & Kunz 2012) and it is consistent with the simulations presented in Section 5.

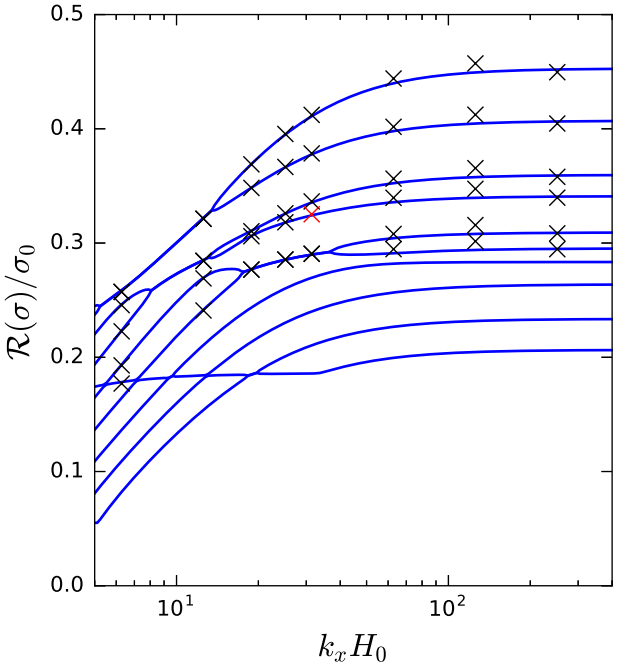

Figure 3. Growth rates as a function of the horizontal wavenumber, k_x, for the 10 fastest growing modes. The solid blue lines were obtained using the pseudo-spectral method. Each cross corresponds to a simulation were the eigenmodes were used for initial conditions. The numerical growth rate was found from the subsequent exponential evolution.

confirmed with the results of the full quasi-global analysis.

4.3. *Solutions obtained with Athena*

We have modified the publicly available MHD code Athena (Stone et al. 2008) in order to be able to describe the nonlinear evolution of weakly-collisional atmospheres with non-uniform composition. Our modified version of the code has anisotropic heat conduction and diffusion of composition with spatially dependent transport coefficients. These modifications, along with tests, were described in detail in Berlok & Pessah (2016) and applied to local settings, where the vertical extent of the simulation domains considered was small compared to the relevant scale-height.

We use a pseudo-spectral method in order to test the numerical solutions obtained with Athena in a quasi-global setting. This is done by exciting the HPBI in the Athena simulations using an exact eigenmode found in the quasi-global linear theory. An example is shown in Figure 4 where four of the components of the perturbation are shown for the $n = 5$ and $m = 4$ mode at $t = 3$ in units of $t_0 = H_0/v_{0,\mathrm{th}} = 45$ Myr. The growth rate is measured in the simulation by following the evolution of the amplitude of the perturbations. We find that the error in the growth rate for this simulation is less than a percent compared to the pseudo-spectral linear theory.

We have thoroughly tested this method by running a suite of simulations where we vary the n and m mode numbers. A total of 42 simulations were run with $n = 1$ to 8 and $m = 1$ to 6 with six of the simulations being degenerate[2] in m. A comparison between the growth rates obtained using the pseudo-spectral method and the simulations is shown in Figure 3. In this figure, each cross corresponds to an individual simulation where the eigenmode was excited exactly. These simulations were run at half the resolution, 256×512, of the simulations presented in Section 5 in order to expedite the numerical simulations. As noted already by Latter & Kunz (2012), the low resolution causes some discrepancy at the highest wavenumbers. These tests illustrate the generally good agreement between the numerical implementation in Athena and our quasi-global linear theory using pseudo-spectral methods.

[2] They are complex conjugate solutions so the eigenvalues do differ in their imaginary part which is however very small.

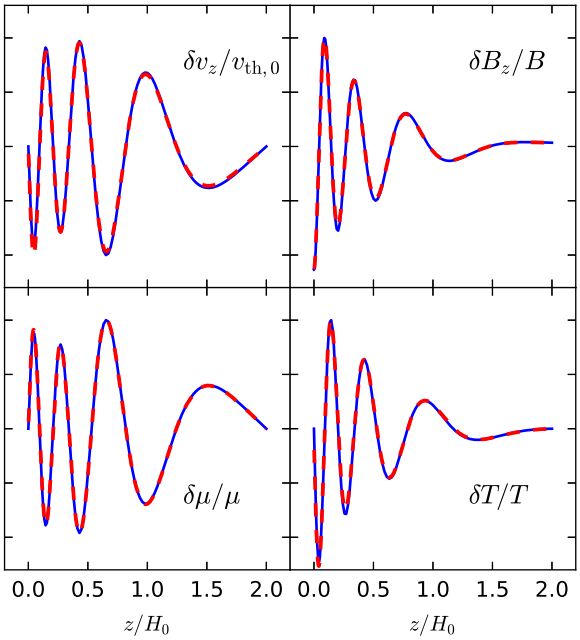

Figure 4. A comparison between a simulation using Athena and the pseudo-spectral method. A slice in the x-direction at $t = 3$ is shown in dashed red and the pseudo-spectral solution is shown in blue. The growth rate is $\sigma/\sigma_0 = 0.324$ according to the pseudo-spectral method and $\sigma/\sigma_0 = 0.325$ according to the simulation, the error is less than a percent. This mode has $n = 5$ and $m = 4$ and it is also indicated with a red cross in Figure 3.

5. INNER REGIONS OF THE ICM

In this section we consider the long time evolution of plasma instabilities in the inner regions of the ICM by performing fully nonlinear simulations of the HPBI using Athena. We describe the details of the numerical setup in Section 5.1, the evolution of key quantities in Section 5.2 and conclude by comparing a simulation of the HPBI with a simulation of the HBI in Section 5.3.

Some of the simulations include Braginskii viscosity which is a numerical and theoretical challenge (Schekochihin et al. 2005; Kunz et al. 2012). The reason is that microscale instabilities are triggered if the magnitude of the pressure anisotropy grows too large. The pressure tensor can become anisotropic due to conservation of the first adiabatic invariant of the ions. Specifically, when the pressure anisotropy exceeds the limits given by

$$-\frac{B^2}{4\pi} < p_\perp - p_\parallel < \frac{B^2}{8\pi}\,. \tag{35}$$

the firehose or mirror instabilities are triggered (Parker 1958). This is an issue for the kind of simulations we consider because the microscale instabilities are not correctly described by Braginskii-MHD (Schekochihin et al. 2005).

Two different approaches used to handle this problem are described in Kunz et al. (2012). The first approach is to use high resolution and hope that the firehose instability grows sufficiently fast in order to regulate the pressure anisotropy. The second approach is to artificially limit the pressure anisotropy to the interval given by Equation (35). The latter approach is motivated by studies showing that the microscale instabilities will likely saturate by driving the pressure anisotropy back to marginal stability (Schekochihin et al. 2008; Bale et al. 2009; Rosin et al. 2011) and a similar approach has been used for the magnetorotational instability in local studies of weakly collisional disks (Sharma et al. 2006). A recent study of the solar wind showed that the firehose and mirror thresholds also provide good constraints for the pressure anisotropy in a multi-species plasma with electrons, hydrogen and helium ions (Chen et al. 2016). We have used both of these approaches in our simulations.

5.1. *Description of numerical setup and overview of results*

We perform a suite of three simulations of the HPBI: one without Braginskii viscosity (HPBI_isoP), one with Braginskii viscosity where the pressure anisotropy is limited (HPBI_Blim) by Equation (35) and one with Braginskii viscosity without limiters (HPBI_Brag). We furthermore consider a simulation where the atmosphere has uniform composition ($c_0 = c_Z = 0.62$) in order to compare the simulations with the homogeneous case (HBI_Brag) in Section 5.3.

The initial condition is the plane-parallel atmosphere introduced in Section 3. The instability is triggered by adding Gaussian, subsonic noise in the velocity components with a magnitude of 10^{-4}. All simulations have a spatial extent of $H_0 \times 2H_0$ (with $H_0 = 1$ in code units). The resolution used is 512×1024. In terms of the dimensionless units introduced above, the coefficients for anisotropic heat diffusivity and Braginskii viscosity are $\kappa_\parallel = 1.4 \times 10^{-2}\ T^{5/2}\mu\rho^{-1}$ and $\nu_\parallel = 2.6 \times 10^{-4}\ T^{5/2}\rho^{-1}$.

The three simulations of the HPBI are shown in Figure 5 where the evolution of the mean molecular weight and the magnetic field lines is followed as a function of time with snapshots at $t/t_0 = 0$, 25, 40, 100 and 200, with $t_0 = H_0/v_{0,\mathrm{th}} = 45$ Myr. In this figure, a high (low) concentration of helium is indicated with green (purple) and the magnetic field lines are shown as solid black lines. The top row of panels was created from HPBI_isoP which did not include Braginskii viscosity while the middle row (HPBI_Blim) and bottom row (HPBI_Brag) of panels did include Braginskii viscosity.

The various panels in Figure 5 illustrate how the magnetic field, which is initially vertical, becomes rapidly tangled. The temperature profile, which is not shown here does not vary significantly as time progresses. The composition evolves rapidly with bubbles of helium sinking down to the center of the core. By the end of the simulation, the helium content has been very well mixed in HPBI_isoP. In HPBI_Brag blobs of gas with a high helium content have sunk towards the center of the cluster but they have retained their structure and have not mixed with their new environment. This lack of mixing can be understood from the ability of Braginskii

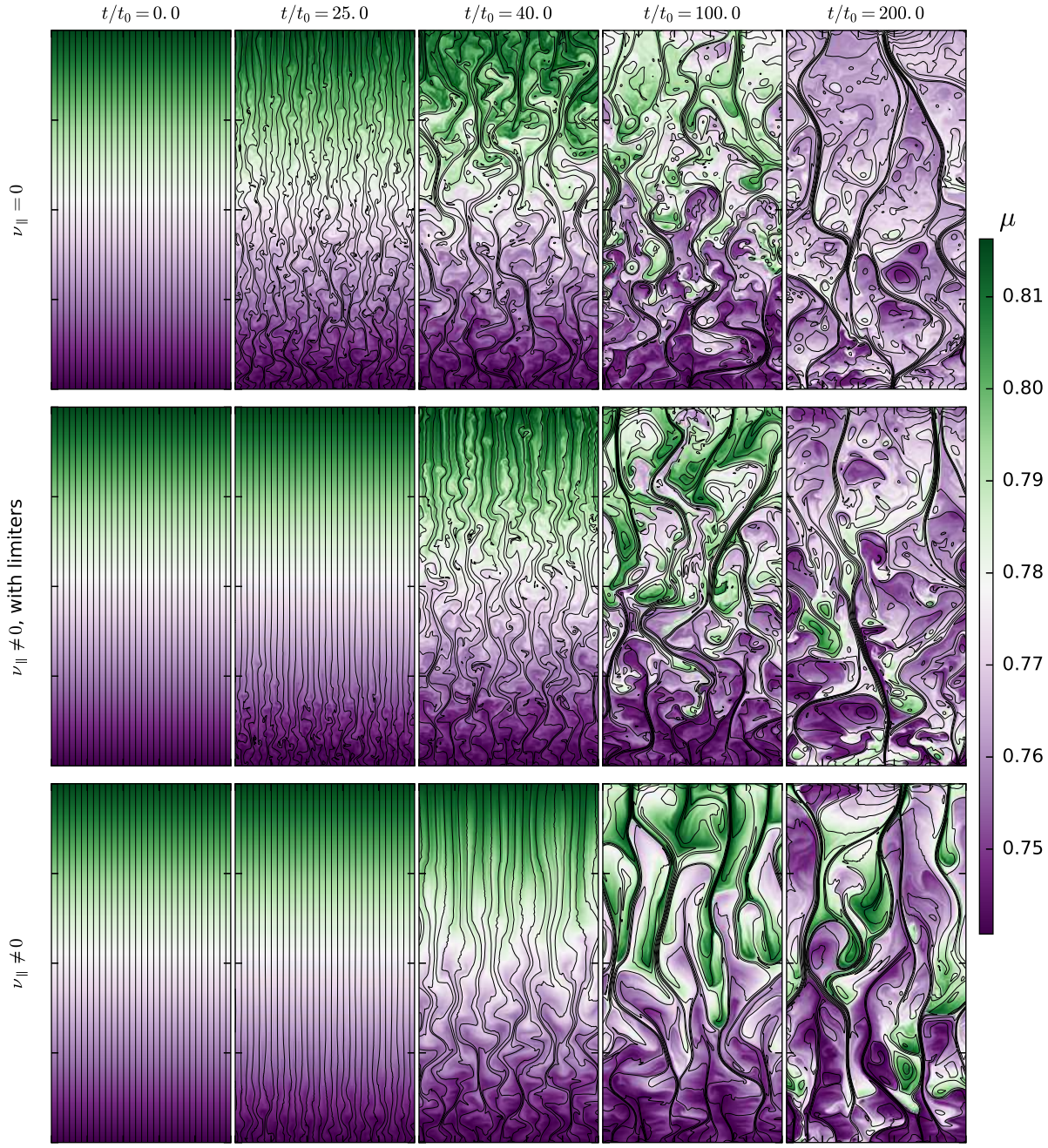

Figure 5. Evolution of the HPBI as a function of time in units of $t_0 = H_0/v_{0,\mathrm{th}} = 45$ Myr. The size of the box is $H_0 \times 2H_0$ with $H_0 = 40$ kpc. The bottom of the atmosphere has $T_0 = 5.8$ keV and $c_0 = 0.52$ while the top of the atmosphere has $T = 9.6$ keV and $c = 0.62$, values found at $r_0 = 160$ kpc and $r = r_0 + 2H_0 = 240$ kpc in the model of Peng & Nagai (2009). The top row of panels include anisotropic heat conduction and the middle and bottom rows also include Braginskii viscosity. The middle row uses limiters. An animated version is available at this http URL.

viscosity to make the magnetic field retain a coherent structure over larger distances than one would find for a simulation with isotropic pressure (see the discussion of the MTI in Kunz et al. 2012). This feature, along with the fact that the magnetic field is tied to the gas, suppresses small scale mixing of the helium content. This implies that the spatial distribution of helium might be more patchy in a viscous ICM than in a non-viscous ICM.

5.2. *Evolution of composition, temperature, magnetic field inclination, and energy densities*

The evolution of the composition gradient can be illustrated by taking averages along the x-direction, designated by the brackets $\langle\rangle_x$. This is shown in the top row of panels in Figure 6, which have been produced at the same times as the snapshots shown in Figure 5. We see that on very long timescales of the order of 9 Gyr ($t/t_0 = 200$) the instability,

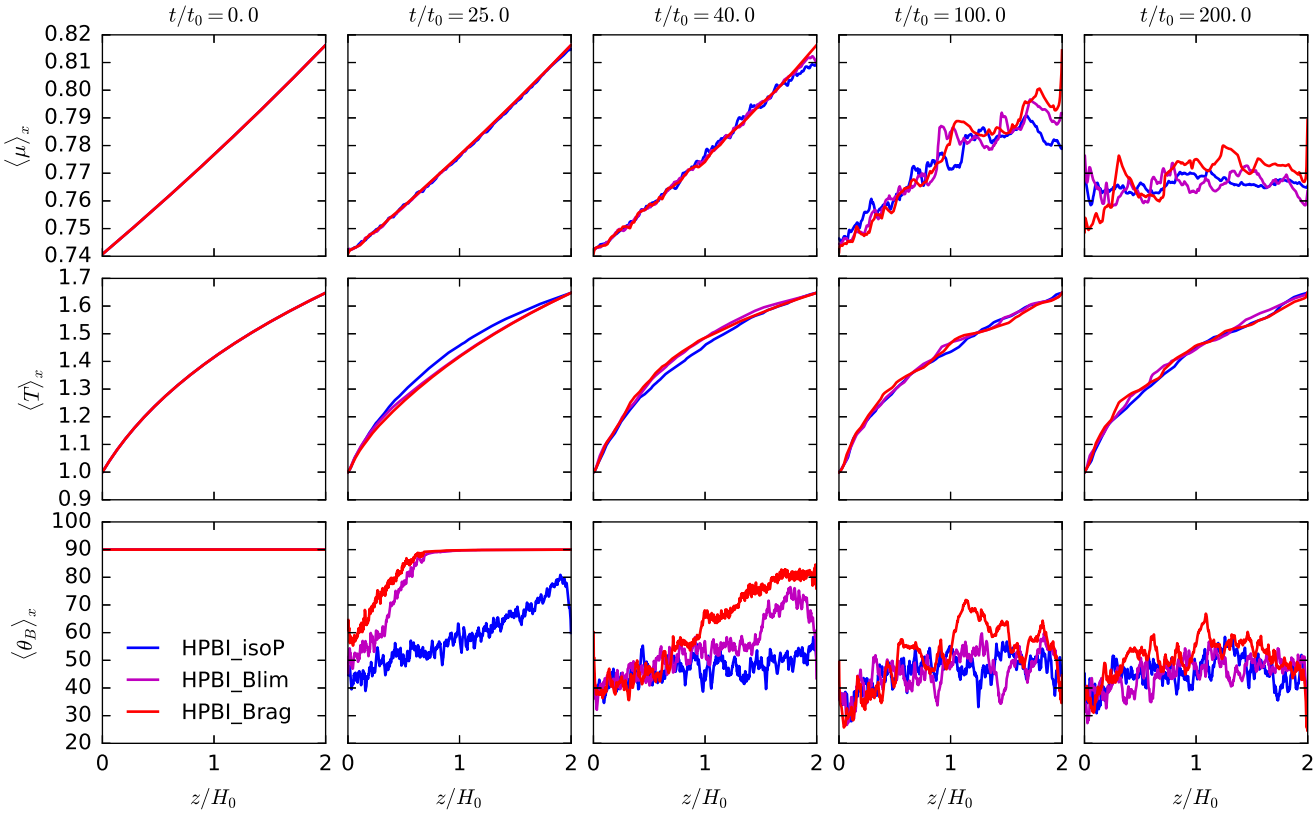

Figure 6. Key quantities averaged along x as a function of height z scaled by $H_0 = 40$ kpc, at times $t/t_0 = 0$, 25, 40, 100 and 200, with $t_0 = 45$ Myr, for the simulation without viscosity (blue), with viscosity and limiters (magenta) and with viscosity but without limiters (red). *Top:* Average mean molecular weight. *Middle:* Average temperature. *Bottom:* Average inclination angle of the magnetic field.

on average, acts to remove the gradient in composition that originally gave rise to it. Note, however, that the gradient in composition is rather long-lived as its profile remains rather unaltered until about 4.5 Gyr ($t/t_0 = 100$).

The evolution of the temperature gradient is less dramatic, as illustrated in the middle row of panels in Figure 6. Changes in the temperature profile are also modest when the composition is uniform, as seen in, for instance, Kunz et al. (2012) and Figure 8.

It is already evident from Figure 5 that the magnetic field changes its inclination with respect to the direction perpendicular to gravity as time progresses. This can be further studied by considering the average inclination angle defined by (Parrish & Quataert 2008)

$$\langle\theta_B\rangle_x = \langle\sin^{-1}(|b_z|)\rangle_x. \tag{36}$$

The evolution of this quantity is shown in the bottom row of panels in Figure 6. We see that the instability grows fastest at the bottom of the atmosphere but increases its region of influence as time progresses. The evolution of $\langle\theta_B\rangle_x$ is initially fast compared with the changes in either composition or temperature and the average angle has changed significantly at most heights by 1.8 Gyr ($t/t_0 = 40$)[3]. However, on timescales of the order of 4.5 Gyr ($t/t_0 = 100$), $\langle\theta_B\rangle_x$ seems to settle at around $\sim 30-50^\circ$ and the overall distribution of angles shows little evolution until the end of the run at 9 Gyr ($t/t_0 = 200$). The change in average inclination angle might have consequences for the cooling flow problem (Fabian 1994) because heat transport is primarily along magnetic field lines. We discuss this in more detail in terms of the Spitzer parameter below.

We consider the evolution of the the kinetic and magnetic energy densities by calculating volume averages, designated by the brackets $\langle\rangle$, and shown in Figure 7 as a function of time. Braginskii viscosity acts to inhibit the growth rate of the instability and we therefore see the highest growth rate in HPBI_isoP, followed by HPBI_Blim (which is less viscous than HPBI_Brag due to the limiters) and then HPBI_Brag. All the simulations saturate with magnetic and kinetic energy density components in rough equipartition with $B_z^2/8\pi$ having increased by a factor of about ten.

[3] In the second panel of the bottom row, it is evident that Braginskii viscosity slows down the instability.

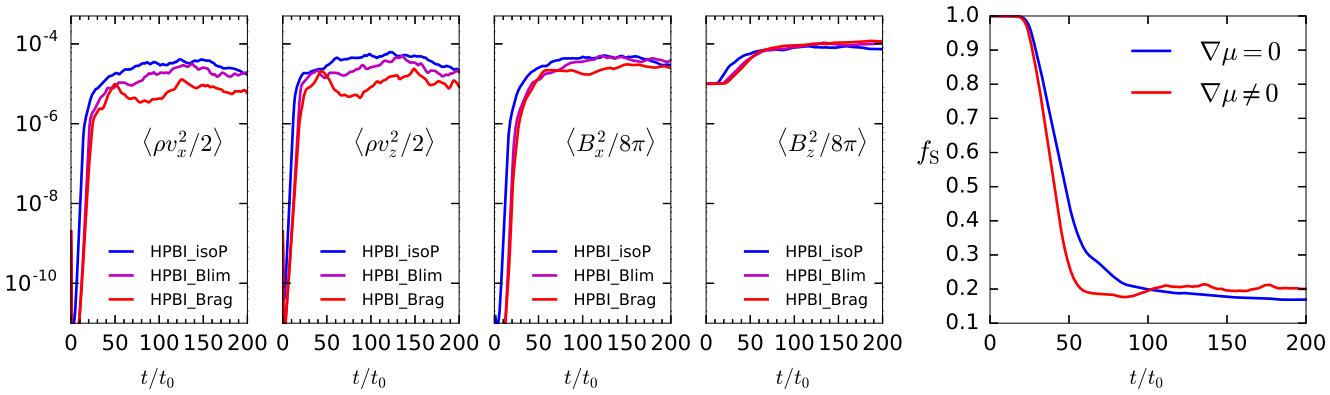

Figure 7. Evolution of the magnetic and kinetic energies in the simulations of the HPBI with blue (HPBI_isoP), red (HPBI_Blim) and magenta (HPBI_Brag) with spatial averages of $\rho v_x^2/2$ (first panel), $\rho v_z^2/2$ (second panel), $B_x^2/8\pi$ (third panel) and $B_z^2/8\pi$ (fourth panel). In the fifth panel we show the evolution of the volume-averaged Spitzer parameter, $f_S = \langle Q_c/\tilde{Q} \rangle$ for the HBI and the HPBI. The initial growth of the HPBI is faster than for the HBI but the final state of the simulation with a composition gradient has a heat flux that is roughly 20 % higher than for the uniform simulation. More information about this panel can be found in Section 5.3.

5.3. *Comparison between HBI and HPBI*

In order to compare our results with previous work on the HBI where the plasma is assumed to be of uniform composition, we performed a simulation (HBI_Brag) using the same atmosphere as for the HPBI but with $c_0 = c_Z$. All other aspects of this simulation are identical to run HPBI_Brag. The evolution of the temperature and the magnetic field is shown in Figure 8. The gradient in composition leads to a slightly faster growth rate with respect to the homogeneous case, as predicted by linear theory (Pessah & Chakraborty 2013; Berlok & Pessah 2015).

We see that both instabilities reorient the magnetic field, driving the average inclination of the magnetic field to be more horizontal (azimuthal). This feature of the HBI has been argued to be of importance for the cooling flow problem because a magnetic field that is predominantly perpendicular to gravity tends to insulate the core from heat transport from the outskirts of the cluster (Parrish & Quataert 2008; Bogdanović et al. 2009; Parrish et al. 2009). For a vertical (radial) magnetic field the heat flux is given by the Spitzer value

$$\tilde{Q} = -\chi_{\parallel} \frac{\partial T}{\partial z} \,, \tag{37}$$

while the heat flux is zero for a horizontal (azimuthal) field. In Berlok & Pessah (2016), we showed that when considering a local domain in an isothermal atmosphere, the HPBI drives the magnetic field to have an average inclination angle of 45°. This is in contrast to the uniform case, where the HBI drives the magnetic field towards 0° (Parrish & Quataert 2008). This feature of the HPBI led us to speculate that a composition gradient might be able to alleviate the cooling flow problem by limiting the average magnetic field inclination. We can now test this idea in our quasi-global simulations where the temperature gradient has been obtained from Vikhlinin et al. (2006).

We consider the evolution of the volume-averaged Spitzer parameter (Parrish & Quataert 2008)

$$f_S = \langle \hat{\boldsymbol{z}} \cdot \boldsymbol{Q}_c/\tilde{Q} \rangle \,, \tag{38}$$

as a function of time. This quantity shows how effective heat conduction is at transporting heat in the radial direction in the cluster compared to the case of a vertical (radial) magnetic field (or unmagnetised heat conduction). The same parameter was used to parameterize the effectiveness of helium sedimentation in the model of Peng & Nagai (2009). We show the evolution of f_S in the fifth panel of Figure 7 with the HBI simulation ($\nabla\mu = 0$) indicated with a blue solid line and the HPBI simulation ($\nabla\mu \neq 0$) indicated with a red solid line. Initially, the volume-averaged Spitzer parameter decreases more rapidly in the HBPI simulation than in the HBI simulation, the reason being the slower growth rate in the absence of a composition gradient. The inclusion of a composition gradient however leads to an increase in the volume-averaged Spitzer parameter at late times compared to the homogeneous case. We find that $f_S \approx 0.20$ ($f_S \approx 0.17$) for the HPBI (HBI) at $t/t_0 = 200$. This corresponds to an increase in heat flux by $\sim 20\%$ with respect to the homogeneous case. Albeit this effect is small, our simulations show that composition gradients could play a part in determining to what extent the inner ICM is thermally shielded from its surroundings.

6. OUTER REGIONS OF THE ICM

In this section, we consider two simulations of the outer parts of the ICM where we assume that the initial magnetic field is perpendicular to gravity, i.e., horizontal. In one of these simulations, labeled MTI_Brag, the plasma is assumed to have uniform composition and in the other one, labeled MTCI_Brag, the composition is assumed to decrease with height (radius). The bottom of the model plane-parallel atmosphere is located at $r = 0.65$ Mpc, corresponding roughly to the radius indicated with an *A* in Figure 8 in Berlok & Pessah (2015).

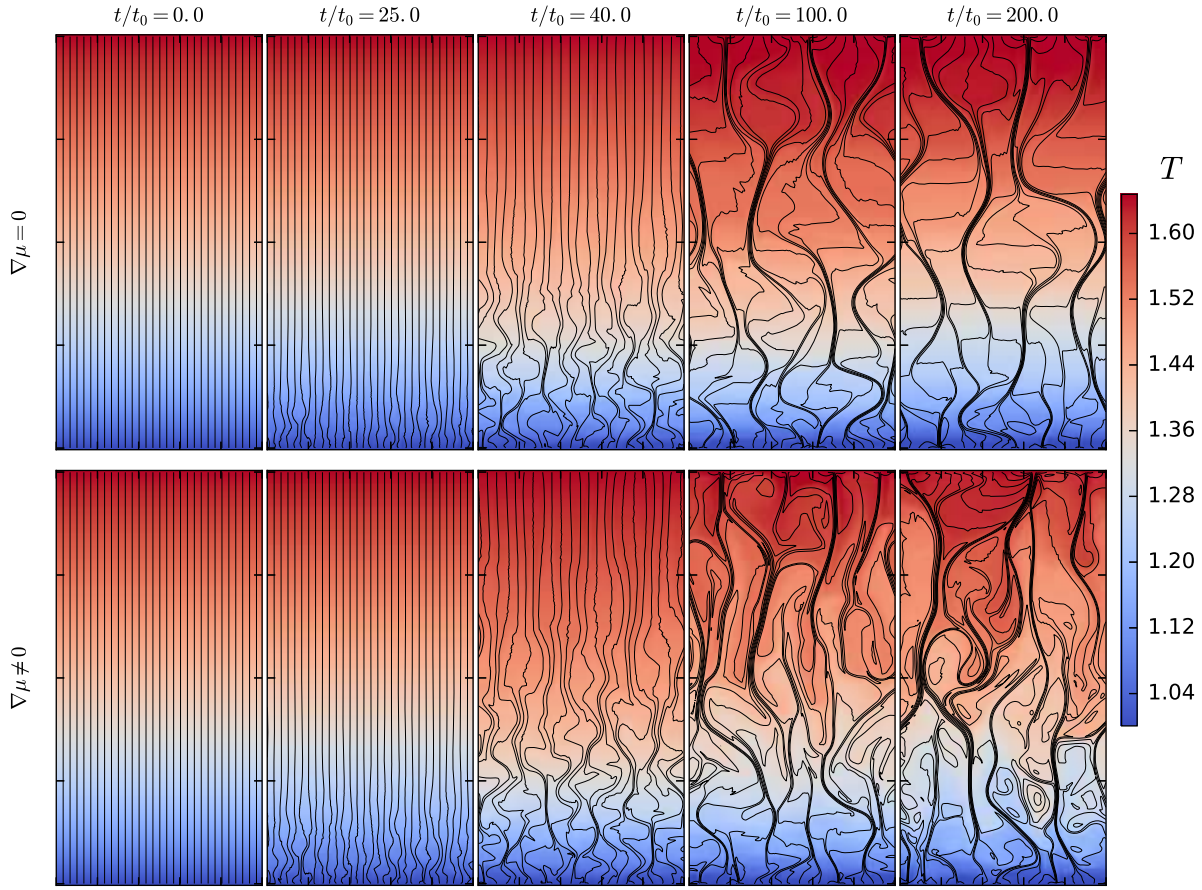

Figure 8. Temperature and magnetic field evolution as function of time for the HBI (HBI_Brag, upper row) and the HPBI (HPBI_Brag, lower row) in units of $t_0 = H_0/v_{0,\rm th} = 45$ Myr. The size of the box is $H_0 \times 2H_0$ with $H_0 = 40$ kpc. The evolution of the composition for HPBI_Brag is shown in the bottom row of Figure 5 while HBI_Brag has uniform composition at all times. Both simulations included anisotropic heat conduction and Braginskii viscosity without limiters.

As in Section 5, we use reflecting boundary conditions at the top and bottom of the domain. The MTCI creates vertical motions that will eventually reach the top and bottom of the domain, potentially influencing the nonlinear evolution of the instability. In order to circumvent this problem, we implement a procedure that has successfully been applied to the MTI by Parrish & Stone (2007) and Kunz et al. (2012). We sandwich the unstable layer between two buffer zones in which we add isotropic heat conduction and viscosity in order to damp any motions making their way into these regions. This results in two stable layers at the top and bottom where the density decreases exponentially away from the mid-plane and the temperature and composition are constant, with values T_0 and c_0 (T_Z and c_Z) in the lower (upper) stable layer.

We use the equilibrium for an initially horizontal magnetic field given in Berlok & Pessah (2016), i.e., the temperature and composition profiles given by

$$T(z) = T_0 + s_{\rm T}\, z' \,, \tag{39}$$

$$c(z) = c_0 + s_{\rm c}\, z' \,, \tag{40}$$

in the middle of the computational domain ($z' = z - H_0/4$ and $H_0/4 < z < 3H_0/4$) where $s_{\rm T} = (T_Z - T_0)/H_0$ is the slope in temperature and $s_{\rm c} = (c_Z - c_0)/H_0$ is the slope in composition. The pressure in the unstable region is given by

$$P(z') = P_0 \left(\frac{T(z')\,\mu(z')}{T_0\,\mu_0} \right)^{\alpha} \,, \tag{41}$$

where $\mu(z)$ is related to $c(z)$ by Equation (4) and the constant coefficient α is given by

$$\alpha = -\frac{T_0}{H_0} \left(\frac{4}{4 s_{\rm T} + 5\mu_0 T_0 s_{\rm c}} \right) \,. \tag{42}$$

Due to the very strong time-step constraint arising from the non-ideal terms, we have however opted to use significantly reduced values of $\chi_\parallel$ and $\nu_\parallel$, by dividing the expected values by a factor of ten. The dimensionless values used in the simulations are therefore $\kappa_\parallel = 0.12\, T^{5/2}\mu\rho^{-1}$ and $\nu_\parallel = 3.3 \times 10^{-3} T^{5/2}\rho^{-1}$. Both temperature and composition decrease with radius with $T_0 = 10.2$ keV and $c_0 = 0.32$ at the bottom of the unstable domain and $T = 9$ keV and $c = 0.27$ at the top for the non-uniform simulation ($c_0 = c_Z = 0.32$ for the uniform simulation). Furthermore, we use $\beta = 10^5$ and include Braginskii viscosity without limiters.

The evolution of the initial horizontal magnetic field and

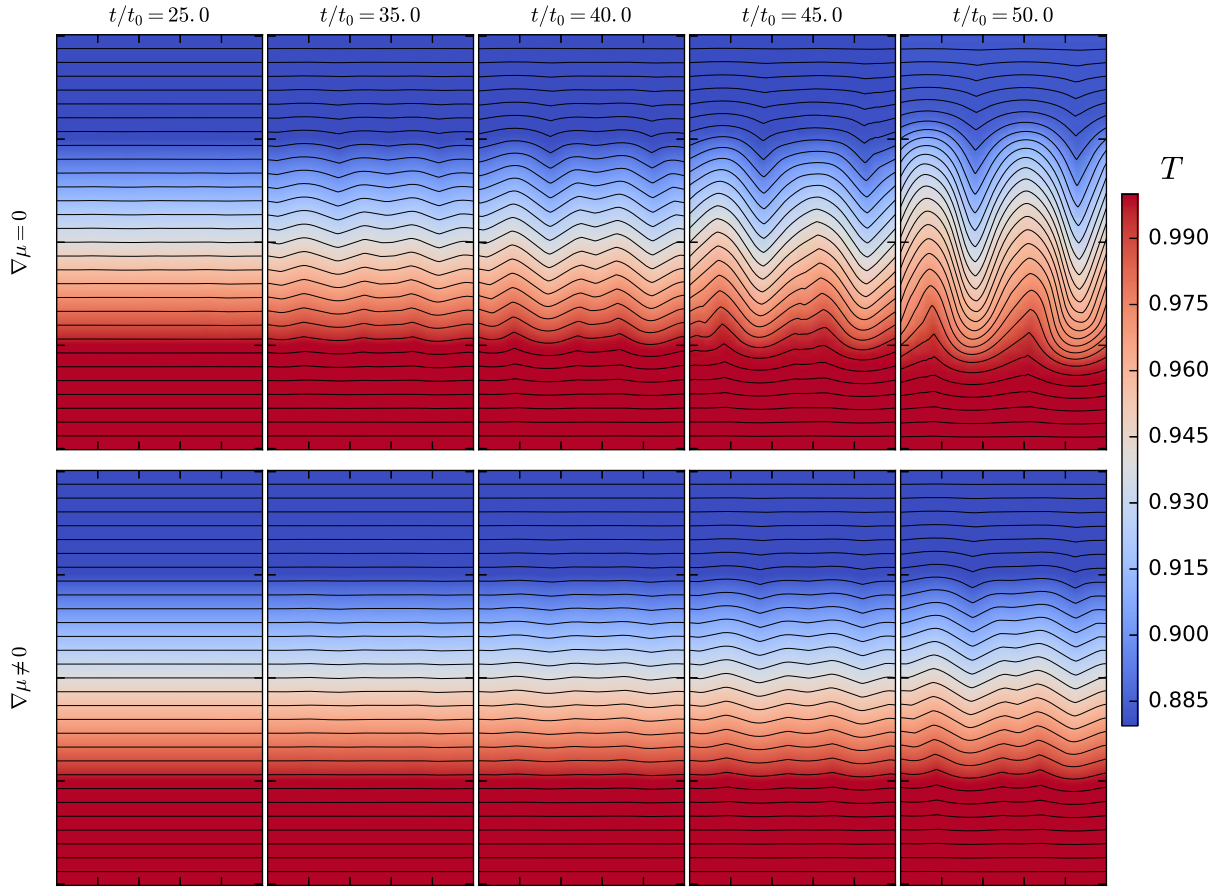

Figure 9. Evolution of the MTI (upper row) and the MTCI (lower row) as function of time in units of $t_0 = H_0/v_{0,\mathrm{th}} = 230$ Myr. The size of the unstable part of the box is $H_0 \times H_0$ with $H_0 = 300$ Mpc. The bottom of the unstable region has $T_0 = 10.2$ keV while the top of the unstable region has $T = 9$ keV, values found at $r_0 = 0.65$ Mpc and $r = r_0 + H_0 = 0.95$ Mpc in the model of Peng & Nagai (2009). The MTI (upper row) has a uniform composition while the MTCI (lower row) has $c_0 = 0.32$ at the bottom and $c = 0.27$ at the top.

the temperature is shown in Figure 9 for MTI_Brag (top row) and MTCI_Brag (bottom row). In these simulations the unit of time is $t_0 = H_0/v_{0,\mathrm{th}} = 230$ Myr. Note that because this is roughly a factor of 5 longer than the t_0 characterising the inner cluster it is only necessary to evolve the simulations up to $50t_0$ to cover timescales of the order of 10+ Gyr. For the MTI (top row) the evolution is very similar to the one presented for the MTI with Braginskii viscosity in Figure 17 in Kunz et al. (2012) except that the growth rate is significantly slower in the simulation presented here. This is simply due to the much shallower temperature gradient that we are using (Vikhlinin et al. 2006). As predicted by theory (Pessah & Chakraborty 2013; Berlok & Pessah 2015), we observe that the instability grows at an even slower rate when a gradient in composition is included (bottom row of Figure 9). For these parameters, linear theory predicts that the maximum growth rate[4] of the MTI is $\sigma = 1.42$ Gyr^{-1} while the MTCI only has a maximum growth rate of $\sigma = 1.09$ Gyr^{-1}. The maximum growth rate is only $\sim 20\%$ slower but this difference is able to significantly alter the final state of the system in this case. The instabilities are still in the exponential phase and have not reached saturation at the end of the simulation.

[4] Found by solving the dispersion relation for a grid of values in k-space and taking the maximum value.

7. DISCUSSION

Understanding the distribution of helium in the intracluster medium is an open problem with important implications for astrophysics and cosmology (Markevitch 2007; Peng & Nagai 2009).

The assumption of a spatially uniform composition of helium in the ICM is routinely applied when interpreting X-ray observations of galaxy clusters. This can lead to biases in the estimates of various key cluster parameters if a composition gradient is present, which can in turn propagate into estimates of the inferred cosmological constants (Markevitch 2007; Peng & Nagai 2009).

Current models to address this problem are one-dimensional and treat the turbulent, magnetized nature of the medium in a very crude way (Fabian & Pringle

1977; Gilfanov & Syunyaev 1984; Chuzhoy & Nusser 2003; Chuzhoy & Loeb 2004; Peng & Nagai 2009; Shtykovskiy & Gilfanov 2010). This usually amounts to parametrize the presence of magnetic fields so that its main effect is to slow down the sedimentation process at the same rate at all radii. The advantage of these kind of models is that they can be evolved for long timescales. In general terms they predict helium profiles that peak off-centre when the (fixed) temperature profile is typical of cool-core clusters (Peng & Nagai 2009).

The approach employed, however, does not allow to take into consideration the fact that the weakly-collisional nature of the ICM renders its properties anisotropic due to inefficient transport across the magnetic field. When the effects of anisotropic heat conduction, viscosity and particle diffusion are considered, with given initial thermal and composition profiles, a wide variety of instabilities, which are absent in one-dimensional settings, can play an important role in the plasma dynamics (Balbus 2000, 2001; Quataert 2008; Kunz 2011; Pessah & Chakraborty 2013).

Ideally, it would be desirable to evolve, in a global setting, the system of equations that describes the evolution of the thermal and composition gradients of a weakly-collisional plasma (with initial cosmic composition) in the potential well of a dark-matter halo. In lieu of pursuing this arguably daunting task at once, we have opted to analyze this problem by developing a better understanding of the plasma dynamics using a number of approximations, which can in principle be relaxed in future studies:

i) We have adopted as a working model a binary mixture composed of hydrogen and helium in the kinetic-MHD approximation with Braginskii viscosity (Braginskii 1965; Pessah & Chakraborty 2013). This approach is known to be subject to small-scale instabilities that need to be dealt with appropriately in numerical simulations (Schekochihin et al. 2005; Kunz et al. 2012). The firehose and mirror instabilities can be more accurately captured using hybrid particle-in-cell codes where the ions are treated as particles and the electrons are treated as a fluid (see for instance Kunz et al. 2014). Studies of the firehose and mirror instabilities normally assume a hydrogen plasma. Extending such simulations in order to study the kinetics of a multispecies plasma might therefore give new insights on how to incorporate microscale instabilities in kinetic MHD simulations of binary mixtures.

ii) We have simplified the geometry of the problem by considering a plane-parallel atmosphere. This approach has been applied with success in a wide variety of astrophysical settings. Its accuracy depends on the phenomena under study having radial scales that are smaller than the fiducial radius at which the model is adopted. We have improved on our previous work (Pessah & Chakraborty 2013; Berlok & Pessah 2015, 2016), in which the domain under considerations were local in both radius and azimuth, and developed a quasi-global approach, extending previous work in homogeneous settings (Latter & Kunz 2012; Kunz et al. 2012). This enabled us to consider domains that are not necessarily small compared to the thermal scale height at the fiducial radius.

iii) The helium concentration profile in galaxy clusters is unfortunately not directly observable (Markevitch 2007). In order to construct our model atmospheres we relied on current one-dimensional helium sedimentation models (Peng & Nagai 2009). By considering these as initial conditions, we investigated the evolution of a number of instabilities that feed off the gradients in temperature and composition in the inner regions as well as the outskirts of the ICM. This approach assumes that the timescales for the evolution of the temperature and composition profiles are long compared to the timescales for the instabilities to grow significantly (Berlok & Pessah 2015). While this seems to be a reasonable assumption, the fact that the large scale gradients, from which the instabilities feed off, are unable to evolve prevents us from understanding how the instabilities interact with the processes that drive their evolution at a more fundamental level (Burgers 1969; Bahcall & Loeb 1990).

While our approach cannot directly predict the evolution of the helium distribution in the ICM, we have been able to learn a few interesting things about how composition gradients can influence the dynamics of the weakly-collisional medium.

In the inner region of the ICM, the nonlinear evolution of our model shows that helium rich material, initially at the top of the atmosphere, will fall down onto the inner core of the cluster. The relevant timescale for mixing to occur is of the order of a few Gyrs. It is important to emphasise that this process cannot be attributed to standard convection driven by composition gradients since the Ledoux criterion (Ledoux 1947) is fulfilled in the model atmospheres we employed. The driving mechanism is the generalisation of the heat-flux driven buoyancy instability HBI, which we have termed the heat- and particle-flux-driven buoyancy instability (HPBI). We analysed in some detail the effects that the evolution of the magnetic fields has on the thermal conductivity of the plasma to assess whether composition gradients can alleviate the core insulation observed in homogeneous settings (Parrish & Quataert 2008). Beyond a few Gyrs, the average inclination angle of the magnetic field is close to $\sim 45^\circ$ resulting in an averaged Spitzer parameter higher by about 20% than the value obtained in a corresponding homogeneous simulation. The distribution of composition is more patchy in the simulations where Braginskii viscosity is included because it can inhibit mixing at smaller scales. The main conclusions described here however seem to be rather insensitive to Braginskii viscosity when composition is averaged along the azimuthal direction.

We also investigated the dynamics of the outskirts of the ICM, where both the temperature and the composition are expected to decrease with increasing radius (Vikhlinin et al. 2006; Peng & Nagai 2009). In this case, the mechanism driving instabilities is the generalisation of the magneto-thermal instability (MTI), which we have termed the magneto-thermal-compositional instability (MTCI). The shallower

gradients characterising current models imply that the instabilities evolve slowly and there is not enough time for them to evolve in the strong non-linear regime even after several Gyrs. Therefore, in the outskirts of the cluster, the instabilities are rather inefficient at erasing the composition gradients.

This mismatch between fast growing instabilities in the inner core and rather slow instabilities in the outskirts could imply that compositions gradients in cluster cores might be shallower than predicted by one-dimensional models. One could speculate about the long-term outcome of the interplay between the various competing processes, but it seems to be safer to develop more self-consistent models in which the instabilities can develop in a global setting where the physics driving helium sedimentation is accounted for. One alternative, intermediate step in developing these models could consist of using the type of numerical simulations we have employed here to develop more physically motivated effective models for mixing that can be incorporated in improved one-dimensional models.

The weakly-collisional, magnetized nature of the ICM is likely to have an impact on the long-term evolution of the gas dynamics, including the issue of whether helium can sediment efficiently. Our work constitutes the first few steps in this direction. More quantitative statements will demand improved models that incorporate the physics driving the sedimentation process while simultaneously accounting for the anisotropic transport properties of the medium.

We acknowledge useful discussions with Daisuke Nagai, Matthew Kunz, Prateek Sharma, Ellen Zweibel, and Ian Parrish during the *3rd ICM Theory and Computation Workshop* held at the Niels Bohr Institute in 2014. We would like to thank Matthew Kunz for sharing with us the Athena files used to run the simulations presented in Kunz et al. (2012). Furthermore, we thank him and Henrik Latter for providing us with a copy of the script they used in Latter & Kunz (2012) and that we used as a starting point to build the code used in this paper. We are grateful to Daisuke Nagai and Fang Peng for sharing with us the Fortran program used to calculate the mean molecular weight profile used as inspiration for the simulations presented in this paper. We also acknowledge useful discussions with Gopakumar Mohandas and Sagar Chakraborty. The research leading to these results has received funding from the European Research Council under the European Union's Seventh Framework Programme (FP/2007-2013) under ERC grant agreement 306614. T.B. also acknowledges support provided by a Lørup Scholar Stipend and M.E.P. also acknowledges support from the Young Investigator Programme of the Villum Foundation.

REFERENCES

Bahcall, J. N., & Loeb, A. 1990, ApJ, 360, 267
Balbus, S. A. 2000, ApJ, 534, 420
—. 2001, ApJ, 562, 909
Balbus, S. A., & Potter, W. J. 2016, ArXiv e-prints, arXiv:1603.06489
Bale, S. D., Kasper, J. C., Howes, G. G., et al. 2009, Physical Review Letters, 103, 211101
Berlok, T., & Pessah, M. E. 2015, ApJ, 813, 22
—. 2016, ArXiv e-prints, arXiv:1603.05508
Bogdanović, T., Reynolds, C. S., Balbus, S. A., & Parrish, I. J. 2009, ApJ, 704, 211
Boyd, J. P. 2000, Chebyshev and Fourier Spectral Methods (DOVER)
Braginskii, S. I. 1965, Reviews of Plasma Physics, 1, 205
Burgers, J. M. 1969, Flow Equations for Composite Gases
Carilli, C. L., & Taylor, G. B. 2002, ARA&A, 40, 319
Chen, C. H. K., Matteini, L., Schekochihin, A. A., et al. 2016, ApJL, 825, L26
Chuzhoy, L., & Loeb, A. 2004, MNRAS, 349, L13
Chuzhoy, L., & Nusser, A. 2003, MNRAS, 342, L5
Fabian, A. C. 1994, ARA&A, 32, 277
Fabian, A. C., & Pringle, J. E. 1977, MNRAS, 181, 5P
Gilfanov, M. R., & Syunyaev, R. A. 1984, Soviet Astronomy Letters, 10, 137
Gupta, H., Rathor, S. K., Pessah, M. E., & Chakraborty, S. 2016, Physics Letters A, 380, 2407
Kunz, M. W. 2011, Monthly Notices of the Royal Astronomical Society, 417, 602
Kunz, M. W., Bogdanović, T., Reynolds, C. S., & Stone, J. M. 2012, The Astrophysical Journal, 754, 122
Kunz, M. W., Schekochihin, A. A., & Stone, J. M. 2014, Physical Review Letters, 112, 205003
Latter, H. N., & Kunz, M. W. 2012, MNRAS, 423, 1964
Ledoux, P. 1947, ApJ, 105, 305
Markevitch, M. 2007, ArXiv e-prints, arXiv:0705.3289
McCourt, M., Parrish, I. J., Sharma, P., & Quataert, E. 2011, MNRAS, 413, 1295
McCourt, M., Sharma, P., Quataert, E., & Parrish, I. J. 2012, MNRAS, 419, 3319
Parker, E. N. 1958, Physical Review, 109, 1874
Parrish, I. J., McCourt, M., Quataert, E., & Sharma, P. 2012a, MNRAS, 422, 704
—. 2012b, MNRAS, 419, L29
Parrish, I. J., & Quataert, E. 2008, ApJL, 677, L9
Parrish, I. J., Quataert, E., & Sharma, P. 2009, ApJ, 703, 96
—. 2010, ApjL, 712, L194
Parrish, I. J., & Stone, J. M. 2005, The Astrophysical Journal, 633, 334
—. 2007, The Astrophysical Journal, 664, 135
Parrish, I. J., Stone, J. M., & Lemaster, N. 2008, ApJ, 688, 905
Peng, F., & Nagai, D. 2009, The Astrophysical Journal, 693, 839
Pessah, M. E., & Chakraborty, S. 2013, ApJ, 764, 13
Quataert, E. 2008, The Astrophysical Journal, 673, 758
Rosin, M. S., Schekochihin, A. A., Rincon, F., & Cowley, S. C. 2011, MNRAS, 413, 7
Ruszkowski, M., & Oh, S. P. 2010, ApJ, 713, 1332
Schekochihin, A. A., Cowley, S. C., Kulsrud, R. M., Hammett, G. W., & Sharma, P. 2005, The Astrophysical Journal, 629, 139
Schekochihin, A. A., Cowley, S. C., Kulsrud, R. M., Rosin, M. S., & Heinemann, T. 2008, Physical Review Letters, 100, 081301
Schwarzschild, M. 1958, Structure and Evolution of the Stars.
Sharma, P., Hammett, G. W., Quataert, E., & Stone, J. M. 2006, ApJ, 637, 952
Shtykovskiy, P., & Gilfanov, M. 2010, MNRAS, 401, 1360
Spitzer, L. 1962, Physics of Fully Ionized Gases
Stone, J. M., Gardiner, T. A., Teuben, P., Hawley, J. F., & Simon, J. B. 2008, The Astrophysical Journal Supplement Series, 178, 137

Vikhlinin, A., Kravtsov, A., Forman, W., et al. 2006, ApJ, 640, 691